



# Kelvin-Helmholtz instability as one of the key features for fast and efficient emulsification by hydrodynamic cavitation

Žan Boček<sup>a</sup>, Martin Petkovšek<sup>a</sup>, Samuel J. Clark<sup>b</sup>, Kamel Fezzaa<sup>b</sup>, Matevž Dular<sup>a,\*</sup>

<sup>a</sup> Faculty of Mechanical Engineering, University of Ljubljana, Askerceva 6, 1000 Ljubljana, Slovenia

<sup>b</sup> Advanced Photon Source, Argonne National Laboratory, 9700 S Cass Ave, Lemont, IL 6043, USA

## ARTICLE INFO

### Keywords:

Emulsion  
Hydrodynamic cavitation  
Kelvin-Helmholtz instability  
Venturi microchannel

## ABSTRACT

The paper investigates the oil–water emulsification process inside a micro-venturi channel. More specifically, the possible influence of Kelvin-Helmholtz instability on the emulsification process. High-speed visualizations were conducted inside a square venturi constriction with throat dimensions of 450  $\mu\text{m}$  by 450  $\mu\text{m}$ , both under visible light and X-Rays. We show that cavity shedding caused by the instability results in the formation of several cavity vortices. Their rotation causes the deformation of the oil stream into a distinct wave-like shape, combined with fragmentation into larger drops due to cavitation bubble collapse. Later on, the cavity collapse further disperses the larger drops into a finer emulsion. Thus, it turns out that the Kelvin-Helmholtz instability is similarly characteristic for hydrodynamic cavitation emulsification inside a microchannel as is the Rayleigh-Taylor instability for acoustically driven emulsion formation.

## 1. Introduction

Defined as colloidal systems consisting of two immiscible liquids [1] – typically oil and water – emulsions exhibit unique properties that make them indispensable in numerous applications. The ability of emulsions to combine substances that would otherwise remain separate enables the creation of products with enhanced stability [2–4], improved texture [5–8], and controlled release of active ingredients [9–13]. Emulsions play a pivotal role in various industries, serving as versatile and essential formulations in areas such as food, pharmaceuticals, cosmetics, and beyond [14–17].

The preparation of emulsions involves intricate techniques that demand understanding of the physical and chemical characteristics of the components involved [15,18]. Most commonly, techniques such as high-pressure homogenization [19–23], static mixing [24,25], rotor–stator interaction [23,25–28] and finally ultrasonication [25,29–34] are employed to achieve stable and homogeneous emulsions. The latter is mainly associated with the occurrence of the cavitation phenomenon and produces a more homogenous emulsion while requiring less energy, maintenance, smaller amounts of surfactant and lower costs [29,32–38].

Ultrasonic emulsification process is driven by cavitation – the appearance of vapor cavities inside a liquid medium due to an extreme local pressure drop. Generally, such evaporation, can be achieved either

with ultrasound or hydrodynamically, resulting in either acoustic or hydrodynamic cavitation, respectively [39]. These unstable bubbles violently collapse inside regions of increased pressure, while in the process emitting intense shockwaves and creating focused liquid jets [39,40]. This results in extensive noise, damages to solid surfaces and, most importantly for the process of emulsion formation, destabilization and fragmentation of liquid–liquid interfaces [23,31,41–44].

There are many reports on cavitation induced emulsification [10,21–23,25,29–38,41–51], but the vast majority focuses only to the ultrasonically driven bubble formation [10,21,29–36,38,51]. In several of our past studies we scrutinized the interaction of the oil–water interface with the cavitation bubbles [31,44,52]. We have remedied the established physics and defined a solid foundation for possible future optimization of the ultrasonic emulsification process (Fig. 1).

Fig. 1 shows the main events during ultrasonic emulsification. As the ultrasonic horn is switched on, cavitation bubbles begin to appear and collapse (Fig. 1a and f), pushing the two liquids into each other, and by doing so, disturbing the interface. The interface begins to deform (Fig. 1b and g) and the instability grows in the so-called linear phase. This will eventually transition into a nonlinear regime, which occurs when the disturbance growth velocity reaches terminal velocity [53,54]. From this point on the interface is destabilized (Fig. 1c and h), leading to the final stage of the Rayleigh-Taylor instability. Emulsion droplets

\* Corresponding author.

E-mail address: [matevz.dular@fs.uni-lj.si](mailto:matevz.dular@fs.uni-lj.si) (M. Dular).

separate from the interface (Fig. 1 d and i) and finally break up to form a homogeneous emulsion (Fig. 1 e and j). For more detail the reader should also refer to [31,43,44,53,54].

Studies on the exploitation of hydrodynamic cavitation for emulsification are scarce. Some exceptions can be found in [11,23,45,46,50,55]. Even more, there is no in-depth report on the physics (or chemistry) of emulsion formation by hydrodynamic cavitation. This is surprising as it has been shown many times that hydrodynamic cavitation is a superior technique to the ultrasonic cavitation in many processes, offering lower energy consumption, higher throughput, continuous operation etc. [23,41,46,56].

The present paper shows observations of the beginning of the emulsion formation, induced at the interaction between the oil stream and the hydrodynamic cavitation structure. As mentioned, hydrodynamic cavitation emulsification was considered before, but it seems that there is one important feature that everyone missed – the formation of the Kelvin-Helmholtz instability at the vapor liquid interface affects the oil stream and consequently emulsification. The reason for previous misinterpretation of the mechanisms may possibly be due to its only recent discovery by the present authors Dular [57]. The physics resembles the Rayleigh-Taylor instability which was similarly found to be characteristic for the ultrasonically driven emulsification process (Fig. 1) [31]. Here a difference in densities is essential for its formation – the thinner liquid being located below the denser one, forcing the former to rise and latter to sink [53,54,58]. Meanwhile, the Kelvin-Helmholtz instability forms at the layer separating two parallelly flowing immiscible fluids with different velocities. This is explained in greater detail below.

The paper is structured as to firstly present a typical cavitation sequence inside the micro-venturi-channel, followed by a detailed description of the Kelvin-Helmholtz instability and its influence on cavity shedding. Based on this discussion and complemented by X-ray measurements in synchrotron, we present and explain the two distinct emulsification mechanisms.

## 2. Experimental set-up

### 2.1. Test section and operating conditions

Emulsions were prepared with distilled water and a mineral hydraulic oil with a density of  $869 \text{ kg/m}^3$  and kinematic viscosity of  $46 \text{ mm}^2/\text{s}$ . The experimental set-up is shown in Fig. 2.

A small gear pump (1) transports distilled water from the reservoir (2) through the  $10 \text{ }\mu\text{m}$  nylon and  $1 \text{ }\mu\text{m}$  glass fiber filter (3). The back-pressure regulator (4) limits the flow on the primary line of the setup, therefore setting the upstream pressure in the test section (5). The stainless-steel sheet (AISI 316L) with a convergent-divergent constriction ( $18^\circ - 10^\circ$ ) is sandwiched between two acrylic glass plates. Oil stream enters the test section from an air-pressurized container (6), just 3 mm upstream of the throat of the Venturi constriction. The emulsified

flow from the test section is discarded (7) in order not to contaminate the set-up by the formed oil–water emulsion. Hence, all emulsification occurs in a single pass through the microchannel. Both channel inlet and outlet are perpendicular to the flow inside the constriction.

Experiments were performed under different operating conditions, e.g. channel dimensions and water and oil pressures. From all results the same conclusions could be reached. For clarity, in the paper we only show results obtained in a venturi constriction that had a height and width of  $450 \text{ }\mu\text{m}$  at an upstream water pressure of 4 bar and oil pressure 6 bar. At these conditions the water mass flow rate was  $6.43 \text{ g/s}$ , corresponding to the flow velocity in the throat of approximately  $31.8 \text{ m/s}$ , leading to Re number of  $\text{Re} = 14300$ , indicating developed turbulent flow regime. The cavitation number, calculated on the basis of upstream pressure and throat velocity [59] was  $\sigma = 0.79$ . The oil flow rate was  $0.65 \text{ g/s}$ .

### 2.2. Visible light visualization

Emulsification was observed with a high-speed camera Photron FASTCAM SA-Z. Whole flow field observations were conducted at 240.000 fps, the fastest available shutter speed of  $0.25 \text{ }\mu\text{s}$  and a resolution of  $512 \times 104$  pixels (approximately  $45.0 \text{ }\mu\text{m}/\text{pixel}$ ). The camera was equipped with a 32 mm macro extension tube and 105 mm AF-S Micro Nikkor lens (Nikon Corporation, Japan). For close-up recordings, the high-speed camera was set to somewhat lower rate of 224.000 fps, the same shutter speed of  $0.25 \text{ }\mu\text{s}$  and a resolution of  $640 \times 96$  pixels (approximately  $21.4 \text{ }\mu\text{m}/\text{pixel}$ ). These observations were done with a 5X Mitutoyo Plan Apo Infinity Corrected Long WD objective (Mitutoyo Europe GmbH, Germany). Back light illumination of venturi section was provided by a Godox Litemons LA200D 5.600 K LED light at 100 % power.

### 2.3. X-ray visualization

In addition to the conventional imaging, we used high speed X-Ray measurements, which can reveal further details of the emulsification process. These were conducted at the Argonne National Laboratory – Advanced photon source (Sector 32-ID-B), which provides a highly intense X-Ray beam with a broad energy spectrum from 7 to 40 keV. Images were captured by a Phantom TMX 6410 high-speed camera with a 10x magnification through a LuAG:Ce scintillator screen with an approximate field of view of  $2.37 \text{ mm} \times 0.36 \text{ mm}$ . The camera resolution was set to  $1280 \times 192$  pixels (approximately  $1.85 \text{ }\mu\text{m}/\text{pixel}$ ) and synchronized with the hybrid APS timing mode at 272.000 fps.

The phase contrast imaging technique, used in the present experiment, relies mainly on the interference between the X-Rays, which are diffracted at the liquid–vapor or liquid–liquid interfaces and the non-diffracted ones. In addition, the light attenuation is related to the material properties the beam passes on its way to the detector – vapor has the smallest attenuation coefficient, oil has a much larger one and water

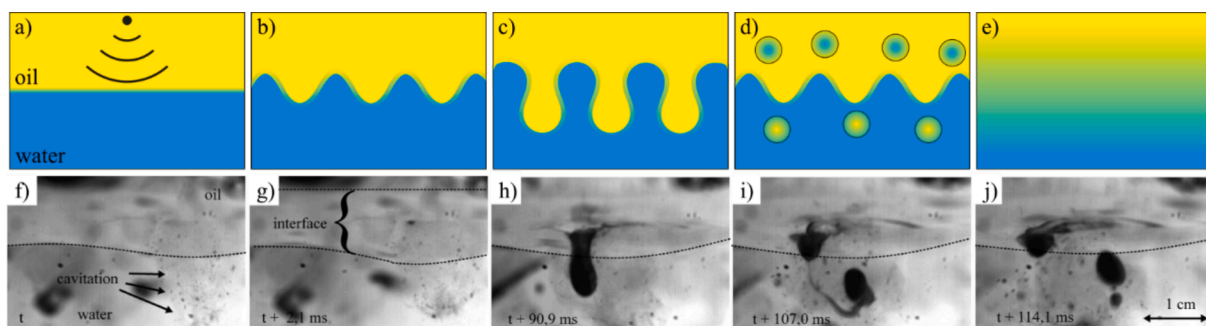


Fig. 1. Ultrasonic emulsification due to Rayleigh-Taylor instability: (a–e) a very much simplified scheme of the process and (f–g) W/O emulsion formation as observed by [31].

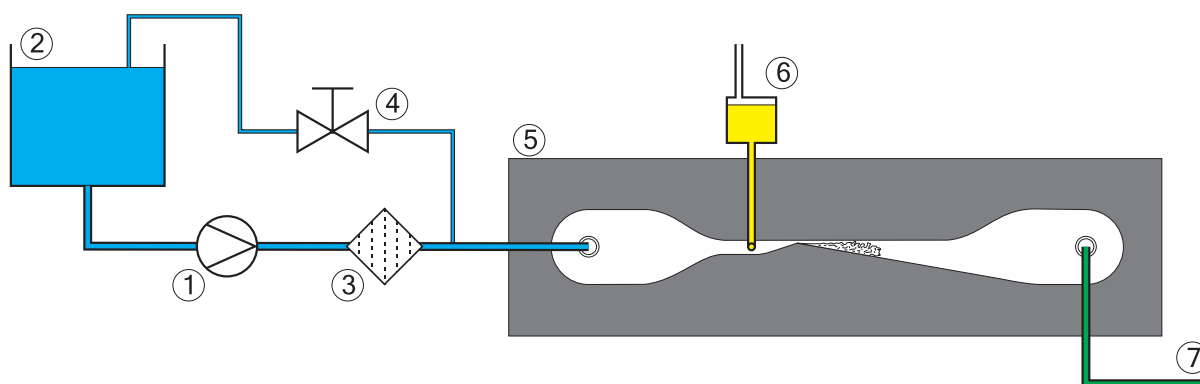


Fig. 2. Experimental setup.

has the highest; hence the bubble will appear the brightest, while oil and water will be darker in the image.

### 2.4. Key experimental parameters and initial conditions

It is well known that in a closely controlled experiment or simulation the initial conditions will play a major role in the development of the instabilities [53]. In the present investigation, however, such control is not possible, mainly due to the stochastic nature of cavitating flow. Nonetheless care was taken in establishing repeatable conditions in terms of water inlet and outlet pressures, oil inlet pressure, flow rate, and finally cavitation number. As already mentioned, the general behavior of emulsification did not significantly differ as the conditions were varied. As this paper is reporting on the newly discovered phenomenon, only one set is shown for the sake of clarity. Table 1 gives the key experimental parameters, while key visualization parameters with the corresponding figures are listed in Table 2.

## 3. Results and discussion

### 3.1. The onset of Kelvin-Helmholtz instability

The regular behavior of cavitation in the micro-venturi channel is presented as a sequence of frames in Fig. 3.

Here we can observe three phenomena: i) the classical cavitation cloud-shedding [60] (Fig. 3, frames 1–6), ii) the attached cavity collapse and formation of individual cavity vortices (Fig. 3, frames 7–12), and iii) the repeated growth of a new cavity (Fig. 3, frames 13–18). In the last frame (13), cavitation appears as a single bubble that stretches along a large part of the divergent part of the section. The state is known as stable supercavitation in larger geometries, while it is subject to continuous cavity shedding from its closure at smaller dimensions [61–63].

In larger geometries and depending on the pressure ratio [64,65], the cavitation cloud shedding occurs either due to the presence of shock waves [64] or the reversed flow [61], also called the re-entrant jet [62]. However, in the case of microchannels, the cavity is constrained, and the ratio between throat and bubble size prevents the reversed flow from peeling of the cavity [57,61,63,66]. The periodical cavity shedding is instead induced by the Venturi sections most recognizable feature, the

Table 1  
Key experimental parameters.

Throat dimension [μm]	Inlet pressure [bar]		Flow rate [g/s]		Flow velocity [m/s]	Reynolds number [/]	Cavitation number [/]
450 × 450	4 <sup>a</sup>	6 <sup>b</sup>	6.43 <sup>a</sup>	0.65 <sup>b</sup>	31.8 <sup>c</sup>	14,300	0.79

<sup>a</sup> Distilled water.

<sup>b</sup> Hydraulic oil.

<sup>c</sup> Calculated at the channel throat.

Table 2

Key visualization parameters with the corresponding figures where the results are presented.

Framerate (×10 <sup>3</sup> )	Field of view [mm]	Resolution	Pixel scale [μm/pixel]	Interval between presented frames [μs]	Corresponding figure
224	13.7 × 2.1	640 × 96	21.4	102.7	Fig. 3
240	23.0 × 4.7	512 × 104	45.0	62.5	Fig. 5
224	13.7 × 2.1	640 × 96	21.4	33.3 35.7	Fig. 6 Fig. 7
272 <sup>a</sup>	2.37 × 0.36	1280 × 192	1.85	14.7	Fig. 8

<sup>a</sup> Visualization with X-Rays.

formation of a Kelvin-Helmholtz instability [57,61]. This can be observed both under visible light and with the assistance of X-Rays (Fig. 4), the latter offering a more detailed observation of the phenomena. Under visible light it can be distinguished as several irregularities or “bumps” along the cavitation cloud’s upper boundary (Fig. 4a). X-Ray visualization reveals the true shape of the instability, namely downstream oriented wave-like pattern (Fig. 4b).

The Kelvin-Helmholtz instability is present at the upper gas–liquid interface and during each cavity shedding cycle it commences from the cavity closure line. It forms when the shear flow at the liquid–vapor interface is significant, which occurs as the cavity growth stagnates [57]. The first step towards the formation of the Kelvin-Helmholtz instability is in small initial perturbations and irregularities. These cause the “corrugation” of the sharp interface between the liquid and vapor phase. With almost stationary cavitation pocket, the flow accelerates above the peaks in the interface (where the gap between the interface and upper channel wall is the smallest) and decelerates in the valleys in the interface (where the gap between the interface and upper channel wall is the largest). The resulting interface waves are in turn subject to a Bernoulli pressure correction [58] – as a result the pressure drops above the peaks and increases in the valleys, what causes further increase in their amplitude. Simultaneously, the shear flow causes the roll-up of the now protruding interface waves (Fig. 4, lower image), which destabilizes the

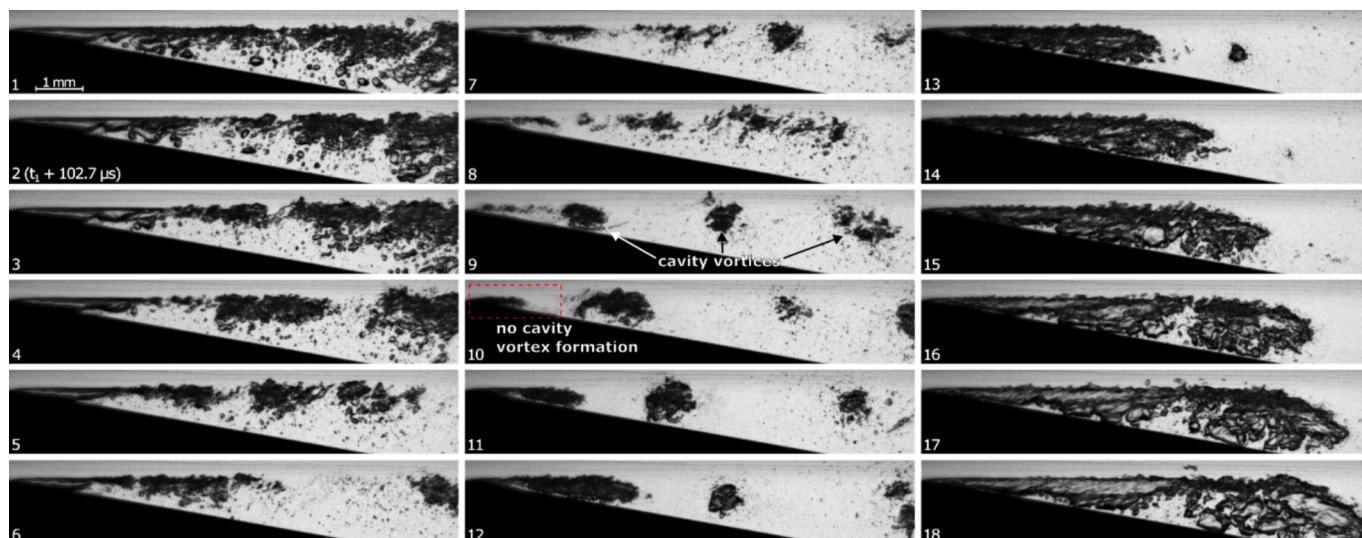


Fig. 3. (Supplemental video 1): Sequence of typical cavity behavior in the venturi microchannel: shedding due to Kelvin-Helmholtz instability, formation of cavity vortices and growth of a new attached cavity (close-up recording under visible light with every 23rd frame shown or 102.7  $\mu\text{s}$  between frames).

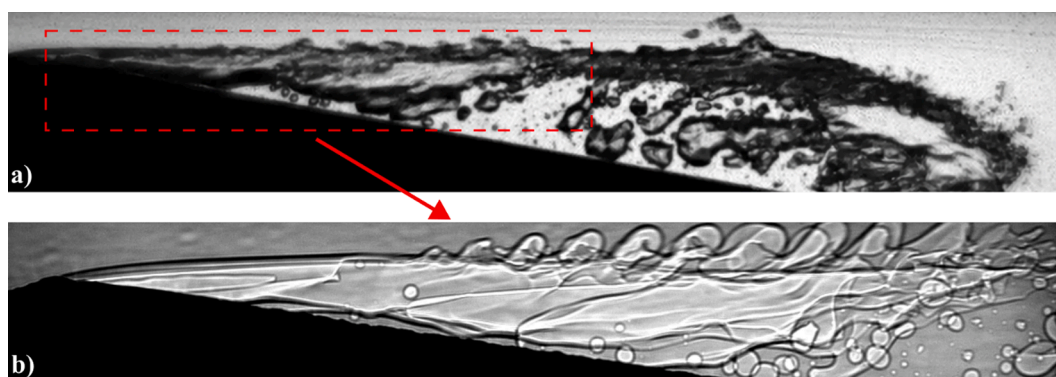


Fig. 4. Kelvin-Helmholtz instability formation on the liquid–vapor interface: close-up recording with (a) visible light and (b) X-Rays (note that these images were not taken simultaneously but rather represent 2 different experiments at the same conditions).

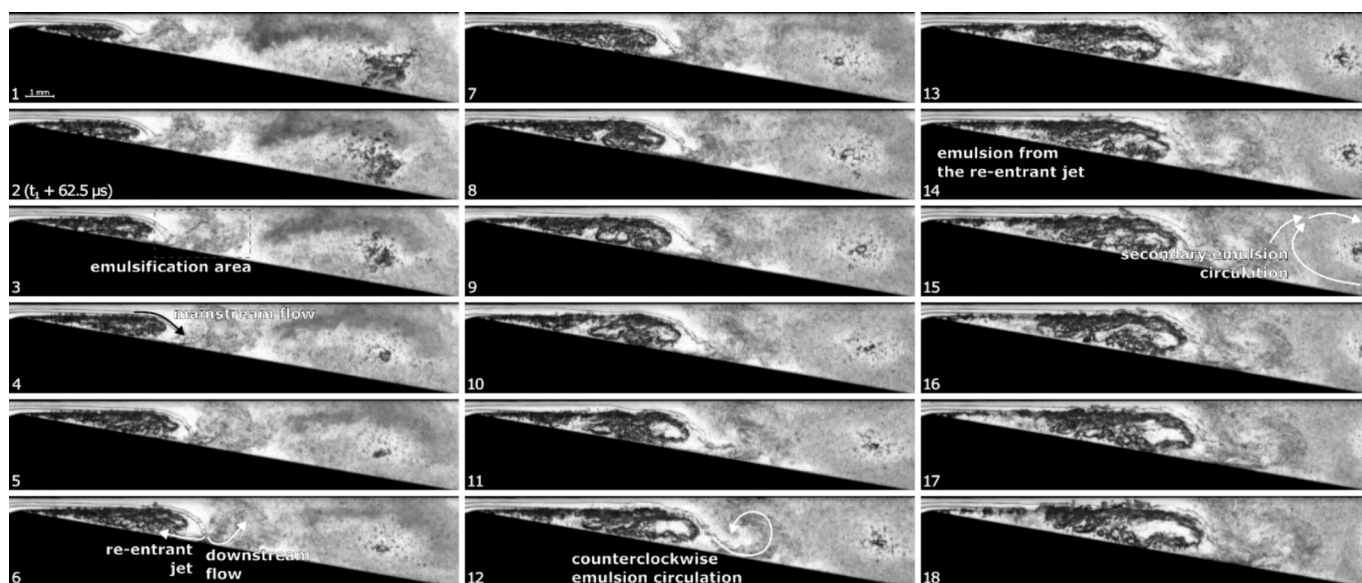


Fig. 5. (Supplemental video 2): Emulsification sequence during the cavity growth phase and prior to the onset of Kelvin-Helmholtz instability (recording under visible light with every 15th frame shown or 62.5  $\mu\text{s}$  between frames).

interface and the attached cavity [67]. The cavity gradually collapses, forming several cavity vortices in the process (Fig. 3, frames 7–12) [57,58,61].

It is important to note that the size of the channel does not play a significant role in the development of the instability as long as it is small enough for the formation of a single attached cavity (supercavitating bubble), however decreasing channel size increases the occurrence probability and the relative size of the Kelvin-Helmholtz instability [57]. For a more detailed discussion on the phenomenon the reader should refer to [57,61,67].

### 3.2. Introduction of oil stream

An oil stream was introduced to the flow, just upstream of the throat of the venturi. One can observe its interaction with the cavitation pocket in Fig. 5.

The entering oil stream flows parallel to the liquid–vapor interface without visible disturbance. During the cavity growth period and prior to the development of the Kelvin-Helmholtz instability the emulsification area is always limited to the sections immediately downstream from the cavity closure (Fig. 5). As it reaches the end of the attached cavity, the oil is directed downwards around the cavity closure (similarly described by Pipp et al. [67]), where emulsion firstly forms (Fig. 5, frames 1–3). No extensive turbulences, which would facilitate the mixing of the oil and water phase, are visible, indicating that cavitation bubble collapse is the predominant mechanism for emulsion formation. Thus, emulsification is most likely confined to downstream of the cavity closure line since smaller cavitation bubbles, which are periodically shed from the attached cavity [57,61], violently collapse in that area [41,63]. The asymmetrical collapse of the cavitation bubbles in the vicinity of the liquid–liquid interface causes the formation of intense shockwaves, micro-jets, and high intensity local microturbulences [23,41–43]. These destabilize the interface and, due to the surface energy of the collapsed bubbles being dissipated at a molecular level, enhance the mixing of immiscible liquids [31,41–44,68]. The larger emulsion drops that are formed during this process are additionally fragmented into smaller droplets [41,42]. This emulsion is carried further by the mainstream flow towards the bottom channel wall, where it visibly separates into the re-entrant jet and downstream flow (Fig. 5, frames 4–6) [60,63,67]. The former, due to the reverse pressure gradient [60], flows upstream and carries some of the formed emulsion towards the constriction (Fig. 5, frames 7–10). This can be confirmed by emulsion droplets visible underneath the attached cavity during later stages of cavity growth (Fig. 5, frames 14–18). Next, when the cavity approaches its maximum length, the mainstream flow carrying the emulsion recirculates counterclockwise downstream of the cavity closure (Fig. 5, frames 11 and 12), ceasing to separate at the bottom channel wall. This vortex is reportedly filled with cavitation bubbles [69], enabling further emulsion formation in and around the vortex, as seen in Fig. 5, frames 13–18. Another recirculating flow can be observed around the following cavity vortex downstream, which rotates opposite to the primary vortex, i.e. clockwise. For a better clarity of the described phenomena the reader should refer to [Supplemental video 2](#). The secondary cavity vortex is a remnant of the previously collapsed attached cavity. The presence of these cavity vortices downstream from the cavity closure line and consequent movement of emulsion is also in accordance with simulation results of Pipp et al. [61,67].

In liquid–liquid flows, where Kelvin-Helmholtz instability forms, it is suspected that at some point the flows will relax toward a self-similar statistical state where the mixing-layer grows as an algebraic function in time [70]. In the present configuration we are dealing also with the presence of cavitation, which exhibits a periodic shedding process at a high frequency, hence even if the self-similarity conditions do exist, they cannot be reached as the cavity will sooner collapse.

As previously described, the shedding caused by Kelvin-Helmholtz instability forms shortly after the cavity reaches its maximum size

[57,60]. Fig. 6 represents the emulsification process inside the microchannel in between the emulsification cycles shown in Fig. 5. We were additionally able to capture these phenomena as the oil stream was first entering the divergent section of the microchannel, enabling a view not obscured by already present emulsion.

From the results shown in Fig. 6 we can firstly note the introduction of an undisturbed oil stream, travelling parallel to the upper liquid–vapor interface (Fig. 6, frame 1–3). This oil stream starts to deform when it reaches a cavity vortex (Fig. 6, frames 4 and 5). In frames 5 and 6 we can observe the onset of emulsion formation, at this time visible as partially transparent droplet clusters originating from the deformed oil stream segments. Additionally in frame 6, the oil stream begins to take a wave-like shape, which becomes elongated and more pronounced in frames 7–11, with more emulsion forming. The wave-like shape of the oil stream translates to the formed emulsion (Fig. 6, frames 12–16). Simultaneously a new attached cavity begins to develop, with the oil stream again flowing undisturbed parallel to the liquid–vapor interface and around the cavity closure line (Fig. 6, frames 17 and 18), similarly to the example of emulsification without the presence of Kelvin-Helmholtz instability (Fig. 5). During this stages emulsification does not occur.

In Fig. 7 we can observe a sequence of frames of the emulsification process induced by the Kelvin-Helmholtz instability.

The oil stream is already present before the described phenomena take place (Fig. 7, frames 1–4), with emulsion from the previously described emulsification mechanism visible downstream from the remaining cavities (Fig. 7, frames 5–9). In frames 10–13 the further shedding and cavity collapse cause the formation of several larger cavity vortices (as reported by Huang et al. [71]), which deform the oil stream and promote emulsion formation. The impingement points of these vortices indicate larger shear stress variations [67], which could, in addition to the emulsion droplet formation induced by cavitation bubble collapse described above, promote emulsification. Hence emulsion formation only takes place near and around these cavity vortices, firstly around the downstream-most vortex (Fig. 7, frames 14–16) and afterwards at the other vortices, in the process forming the emulsion in a wave-like shape (Fig. 7, frames 17–21), as already noted above (Fig. 6, frames 12–16). This close-up angle of observation also offers a better view of the oil stream during the later stages of the process, where the multiple cavity vortices deform it into a distinct wave-like shape (Fig. 7, frames 15 and 16). As a new attached cavity starts to grow (Fig. 7, frames 19–21), the emulsification area is again shifted into the channel section downstream from the cavity closure line.

The same Kelvin-Helmholtz instability induced emulsification was also observed with X-Rays (Fig. 8).

The presented sequence firstly shows the later stages of the instability with the oil stream present in the microchannel (Fig. 8a, frames 1–5). As previously shown (Figs. 5–7) a layer of water is always present between the lower channel wall and the oil stream at the throat of the section. It passes unaffected over the attached cavity and only starts to deform when cavity shedding occurs (Fig. 8a, frames 6–8), during which small cavitation bubbles separate from the main cavity [57,61]. As previously mentioned, the asymmetric collapse of cavitation bubbles near the oil–water interface reduces interfacial tension and promotes emulsification (Fig. 8a, frames 9–12) [23,31,41,46]. Shock waves resulting from symmetric cavity collapse could also reportedly facilitate interface disruption [23], however, Podbevšek et al. [57], using the same microchannel setup, observed their absence. They attributed this to a significant slow-down effect nearby channel walls have on shed cavitation bubble collapse [57]. The oil–water interface disruption hence leads to the appearance of emulsion macrodroplets (Fig. 8a, frames 11–13) [23,45]. Cavitation bubbles and emulsion droplets can be easily differentiated on the synchrotron recordings based on the interface contrast. The macrodroplets are further exposed to cavitation bubbles shed from the cavity, breaking them up into finer emulsion droplets (Fig. 8a, frame 14) [23,45,46,72], circumventing the need for extensive turbulences during hydrodynamic cavitation emulsification

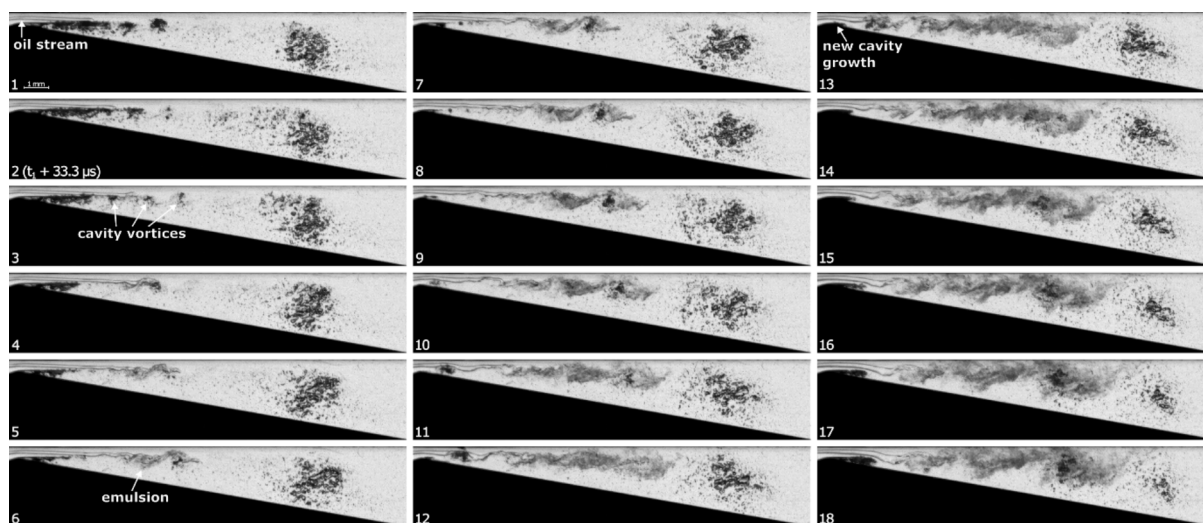


Fig. 6. (Supplemental video 3): Sequence of frames showing the emulsification process induced by Kelvin-Helmholtz instability (recording under visible light with every 8th frame shown or 33.3  $\mu$ s between frames).

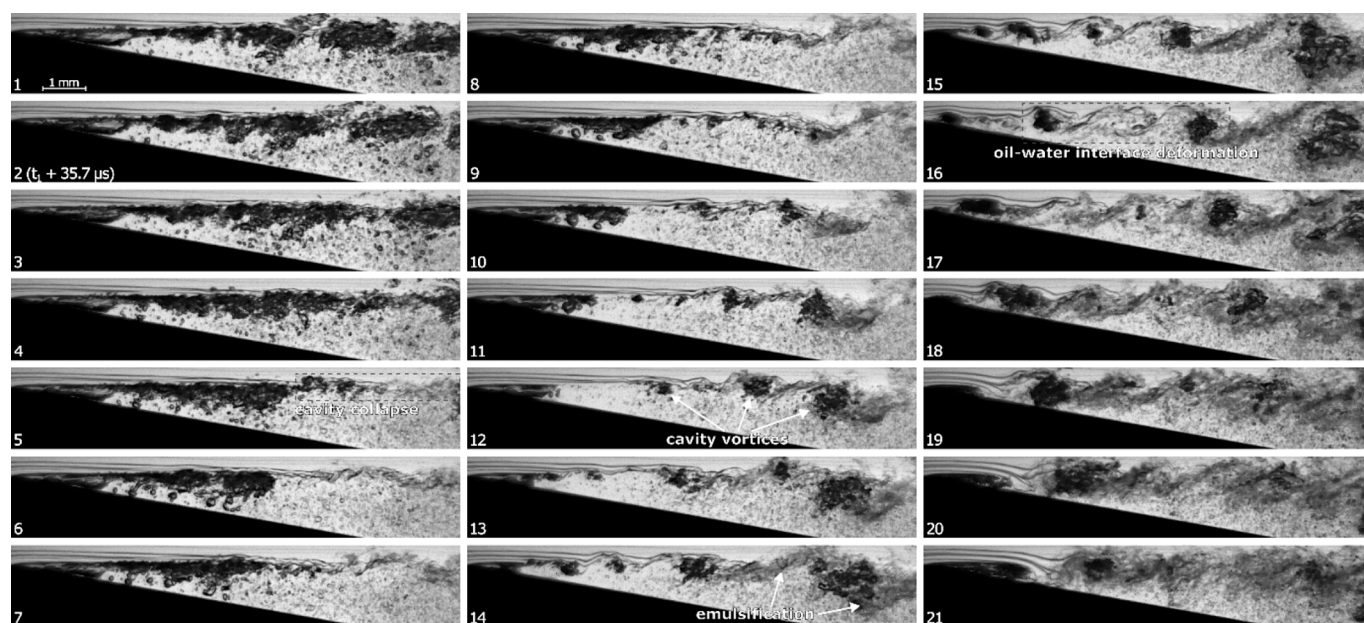


Fig. 7. (Supplemental video 4): Detailed observation of the emulsification process inside the micro-venturi channel: cavitation cloud shedding and oil stream breakup due to Kelvin-Helmholtz instability (close-up recording under visible light with every 8th frame shown or 35.7  $\mu$ s between frames).

[23]. Furthermore, the complete cavity shedding leads to the formation of cavity vortices (Fig. 8a, frame 15) as observed under visible light (Fig. 6, frame 3 and Fig. 7, frame 12). Their clockwise rotation causes additional oil–water interface disruption into the above-described wave-like shape (Fig. 8a, frames 15 and 16). This promotes the breakage of elongated oil stream segments into the water phase (Fig. 8a, frame 17). The macrodroplets are then broken up by cavitation bubbles into smaller droplets with an average diameter of several ten  $\mu$ m (Fig. 8a, frames 18–21, size estimated from these frames), classifying this as a macro-emulsion [34,37,47,48]. Comparing the sequences first and last frame (Fig. 8b), a noticeable increase in emulsion droplet number and decrease in average droplet size can be observed.

#### 4. Conclusions

In our research we demonstrated that oil–water emulsification in a micro-venturi-channel follows two visually distinct pathways. The first

occurs downstream from the cavity closure line and the second at the upper liquid–vapor interface. The former is caused by the mainstream flow inside the channel, carrying the oil stream around the cavity closure. There, smaller cavities, which are shed from the main cavity, collapse, destabilizing the oil–water interface and promoting fluid mixing. The second emulsification mechanism is induced by the formation of a Kelvin-Helmholtz instability (Fig. 9), a feature unique to smaller dimension venturi devices.

The instability forms at the shear layer of the liquid–vapor interface, causing cavity shedding and collapse in the form of larger cavity vortices. These deform the entering oil stream into a wave-like shape, increasing the interfacial area between the oil and water phase, thus increasing the effectiveness asymmetrical cavity collapse has on the emulsification process. The number of collapsing cavities in close proximity to the oil–water interface is also larger during the Kelvin-Helmholtz instability induced cavity shedding. The observations also noted a lack of local turbulent disruptions during both emulsification

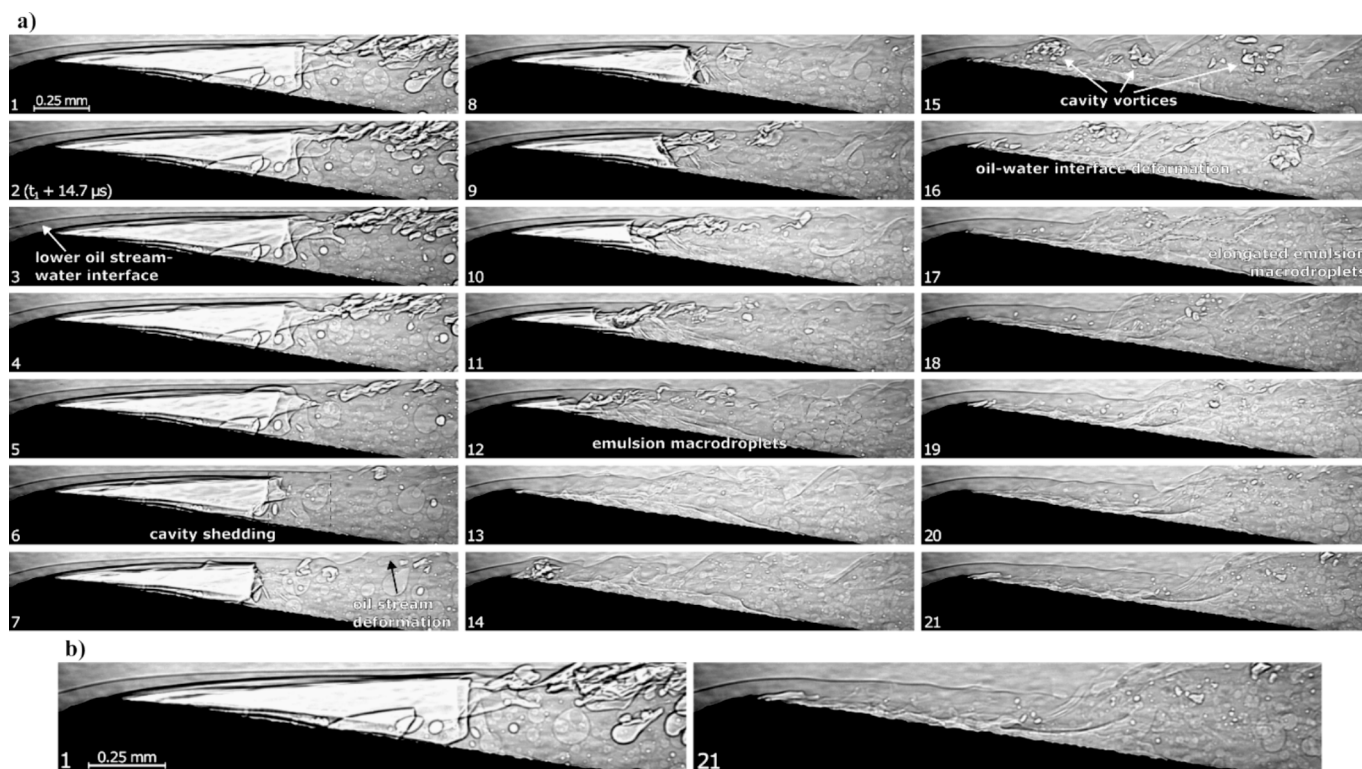


Fig. 8. (Supplemental video 5): (a) Detail on the oil stream breakup and emulsion formation due to the onset of Kelvin-Helmholtz instability with X rays (every 4th frame shown or 14.7  $\mu$ s between frames) and (b) side-by-side comparison of the first and last frame from the sequence.

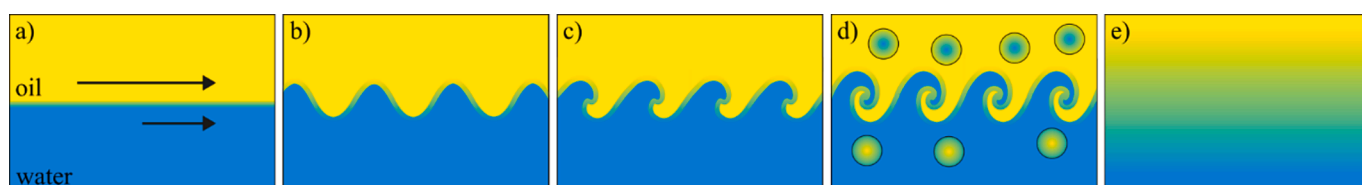


Fig. 9. Emulsification driven by Kelvin-Helmholtz (hydrodynamic cavitation) instabilities – a very much simplified scheme of the process.

pathways, pointing to cavity collapse being the driving force behind emulsification inside the microchannel. The role of the Kelvin-Helmholtz instability during hydrodynamic emulsification is hence comparable to that of the Rayleigh-Taylor instability during acoustic emulsification, necessitating further exploration to pursue the optimization of the process.

**Declaration of competing interest**

The authors declare that they have no known competing financial interests or personal relationships that could have appeared to influence the work reported in this paper.

**Acknowledgments**

The authors acknowledge the financial support from the European Research Council (ERC) under the European Union’s Framework Program for research and innovation, Horizon 2020 (grant agreement n 771567 – CABUM) and the Slovenian Research Agency (Core funding No. P2-0401, P2-0422 and projects No. J2-3044, J2-3057, J2-4480). This research used resources of the Advanced Photon Source, a U.S. Department of Energy (DOE) Office of Science User Facility operated for the DOE Office of Science by Argonne National Laboratory under Contract No. DE-AC02-06CH11357. Finally, the authors also wish to thank

Alex L. Deriy for technical assistance at the Argonne National Laboratory.

**Appendix A. Supplementary data**

Supplementary data to this article can be found online at <https://doi.org/10.1016/j.ultsonch.2024.106970>.

**References**

- [1] T.F. Tadros, Emulsion Science and Technology: A General Introduction, in: Emulsion Science and Technology, 2009: pp. 1–56. <https://doi.org/10.1002/9783527626564.ch1>.
- [2] T. Tadros, P. Izquierdo, J. Esquena, C. Solans, Formation and stability of nano-emulsions, Adv. Colloid Interface Sci. 108–109 (2004) 303–318, <https://doi.org/10.1016/j.cis.2003.10.023>.
- [3] T. Panagiotou, R. Fisher, Improving product quality with entrapped stable emulsions: from theory to industrial application, Challenges 3 (2012) 84–113, <https://doi.org/10.3390/challe3020084>.
- [4] D. Venkataramani, A. Tsulaia, S. Amin, Fundamentals and applications of particle stabilized emulsions in cosmetic formulations, Adv. Colloid Interface Sci. 283 (2020), <https://doi.org/10.1016/j.cis.2020.102234>.
- [5] A.K.D. Santhi, S. Sureshkumar, Factors influencing meat emulsion properties and product texture: a review, Crit. Rev. Food Sci. Nutr. 57 (2017) 2021–2027, <https://doi.org/10.1080/10408398.2013.858027>.
- [6] D.W. Stanley, H.D. Goff, A.K. Smith, Texture-structure relationships in foamed dairy emulsions, 1996.

- [7] J.P.R.J.R.P. V. Lemaitre-Aghazarian P. Piccerelle, M. Sergent, Texture Optimization of Water-in-Oil Emulsions, *Pharm Dev Technol* 9 (2004) 125–134. <https://doi.org/10.1081/PDT-120027424>.
- [8] C. Chung, D.J. McClements, Structure-function relationships in food emulsions: Improving food quality and sensory perception, *Food Struct.* 1 (2014) 106–126, <https://doi.org/10.1016/j.foosr.2013.11.002>.
- [9] T. Mahmood, N. Akhtar, S. Manickam, Interfacial film stabilized W/O/W nano multiple emulsions loaded with green tea and lotus extracts: Systematic characterization of physicochemical properties and shelf-storage stability, *J Nanobiotechnology* 12 (2014), <https://doi.org/10.1186/1477-3155-12-20>.
- [10] S.Y. Tang, M. Sivakumar, Design and evaluation of aspirin-loaded water-in-oil-in-water submicron multiple emulsions generated using two-stage ultrasonic cavitation emulsification technique, *Asia Pac. J. Chem. Eng.* 7 (2012) S145–S156, <https://doi.org/10.1002/apj.664>.
- [11] S.Y. Tang, M. Sivakumar, A novel and facile liquid whistle hydrodynamic cavitation reactor to produce submicron multiple emulsions, *AIChE J* 59 (2013) 155–167, <https://doi.org/10.1002/aic.13800>.
- [12] S.Y. Tang, M. Sivakumar, B. Nashiru, Impact of osmotic pressure and gelling in the generation of highly stable single core water-in-oil-in-water (W/O/W) nano multiple emulsions of aspirin assisted by two-stage ultrasonic cavitation emulsification, *Colloids Surf. B Biointerfaces* 102 (2013) 653–658, <https://doi.org/10.1016/j.colsurfb.2012.08.036>.
- [13] B. Mishra, B.L. Sahoo, M. Mishra, D. Shukla, V. Kumar, Design of a controlled release liquid formulation of lamotrigine, *Daru* 19 (2011) 126–137.
- [14] C. Tan, D.J. McClements, Application of advanced emulsion technology in the food industry: A review and critical evaluation, *Foods* 10 (2021), <https://doi.org/10.3390/foods10040812>.
- [15] J.M. Gutiérrez, C. González, A. Maestro, I. Solé, C.M. Pey, J. Nolla, Nano-emulsions: New applications and optimization of their preparation, *Curr Opin Colloid Interface Sci.* 13 (2008) 245–251, <https://doi.org/10.1016/j.cocis.2008.01.005>.
- [16] C. Solans, P. Izquierdo, J. Nolla, N. Azemar, M.J. Garcia-Celma, Nano-emulsions, *Curr Opin Colloid Interface Sci.* 10 (2005) 102–110, <https://doi.org/10.1016/j.cocis.2005.06.004>.
- [17] M. Chappat, Some applications of emulsions, *Colloids Surf A Physicochem Eng Asp* 91 (1994) 57–77, [https://doi.org/10.1016/0927-7757\(94\)02976-8](https://doi.org/10.1016/0927-7757(94)02976-8).
- [18] G. Narsimhan, Z. Wang, N. Xiang, Guidelines for Processing Emulsion-Based Foods, in: G.L. Hasenhuettl, R.W. Hartel (Eds.), *Food Emulsifiers and Their Applications*, Springer International Publishing, Cham, 2019, pp. 435–501, [https://doi.org/10.1007/978-3-030-29187-7\\_15](https://doi.org/10.1007/978-3-030-29187-7_15).
- [19] S. Schultz, G. Wagner, K. Urban, J. Ulrich, High-Pressure Homogenization as a Process for Emulsion Formation, *Chem. Eng. Technol.* 27 (2004) 361–368, <https://doi.org/10.1002/ceat.200406111>.
- [20] J. Floury, A. Desrumaux, J. Lardieres, L. Lardieres, Effect of high-pressure homogenization on droplet size distributions and rheological properties of model oil-in-water emulsions, 2000.
- [21] Y. Li, D. Xiang, Stability of oil-in-water emulsions performed by ultrasound power or high-pressure homogenization, *PLoS One* 14 (2019), <https://doi.org/10.1371/journal.pone.0213189>.
- [22] B. Freudig, S. Tesch, H. Schubert, Production of Emulsions in High-Pressure Homogenizers – Part II: Influence of Cavitation on Droplet Breakup, *Eng. Life Sci.* 3 (2003) 266–270, <https://doi.org/10.1002/elsc.200390042>.
- [23] J. Carpenter, D.V. Pinjari, V. Kumar Saharan, A.B. Pandit, Critical Review on Hydrodynamic Cavitation as an Intensifying Homogenizing Technique for Oil-in-Water Emulsification: Theoretical Insight, Current Status, and Future Perspectives, *Ind. Eng. Chem. Res.* 61 (2022) 10587–10602, <https://doi.org/10.1021/acs.iecr.2c00754>.
- [24] P. Walstra, Principles of emulsion formation, *Chem. Eng. Sci.* 48 (1993) 333–349, [https://doi.org/10.1016/0009-2509\(93\)80021-H](https://doi.org/10.1016/0009-2509(93)80021-H).
- [25] U. El-Jaby, M. Cunningham, T.F.L. McKenna, Comparison of emulsification devices for the production of miniemulsions, *Ind. Eng. Chem. Res.* 48 (2009) 10147–10151, <https://doi.org/10.1021/ie901005a>.
- [26] K. Urban, G. Wagner, D. Schaffner, D. Röglin, J. Ulrich, Rotor-Stator and Disc Systems for Emulsification Processes, *Chem. Eng. Technol.* 29 (2006) 24–31, <https://doi.org/10.1002/ceat.200500304>.
- [27] A.W. Pacek, S. Hall, M. Cooke, A.J. Kowalski, Emulsification in Rotor-Stator Mixers, in: *Emulsion Formation and Stability*, John Wiley & Sons Ltd, 2013, pp. 127–167, <https://doi.org/10.1002/9783527647941.ch5>.
- [28] U.S. van der Schaaf, H.P. Karbstein, Chapter 6 - Fabrication of Nanoemulsions by Rotor-Stator Emulsification, in: S.M. Jafari, D.J. McClements (Eds.), *Nanoemulsions*, Academic Press, 2018: pp. 141–174. <https://doi.org/10.1016/B978-0-12-811838-2.00006-0>.
- [29] B. Abismail, J.P. Canselier, A.M. Wilhelm, H. Delmas, C. Gourdon, Emulsification by ultrasound: drop size distribution and stability, *Ultrason. Sonochem.* 6 (1999) 75–83, [https://doi.org/10.1016/S1350-4177\(98\)00027-3](https://doi.org/10.1016/S1350-4177(98)00027-3).
- [30] Ž. Boček, M. Petkovšek, S.J. Clark, K. Fezzaa, M. Dular, Dynamics of oil–water interface at the beginning of the ultrasonic emulsification process, *Ultrason Sonochem* (2023) 106657. <https://doi.org/10.1016/j.ultsonch.2023.106657>.
- [31] T. Stepišnik Perdih, M. Zupanc, M. Dular, Revision of the mechanisms behind oil-water (O/W) emulsion preparation by ultrasound and cavitation, *Ultrason. Sonochem.* 51 (2019) 298–304, <https://doi.org/10.1016/j.ultsonch.2018.10.003>.
- [32] S. Mujumdar, S. Kumar, A.B. Pandit, Emulsification by ultrasound: Relation between intensity and emulsion quality, *Indian J. Chem. Technol.* 4 (1997) 277–284.
- [33] A.S. Peshkovsky, S. Bystryak, Continuous-flow production of a pharmaceutical nanoemulsion by high-amplitude ultrasound: Process scale-up, *Chem. Eng. Process.* 82 (2014) 132–136, <https://doi.org/10.1016/j.cep.2014.05.007>.
- [34] C. Yao, S. Zhao, L. Liu, Z. Liu, G. Chen, Ultrasonic emulsification: basic characteristics, cavitation, mechanism, devices and application, *Front. Chem. Sci. Eng.* 16 (2022) 1560–1583, <https://doi.org/10.1007/s11705-022-2160-4>.
- [35] S.M.M. Modarres-Gheisari, R. Gavagsaz-Ghoachani, M. Malaki, P. Safarpour, M. Zandi, Ultrasonic nano-emulsification – A review, *Ultrason. Sonochem.* 52 (2019) 88–105, <https://doi.org/10.1016/j.ultsonch.2018.11.005>.
- [36] S. Kentish, T.J. Wooster, M. Ashokkumar, S. Balachandran, R. Mawson, L. Simons, The use of ultrasonics for nanoemulsion preparation, *Innov. Food Sci. Emerg. Technol.* 9 (2008) 170–175, <https://doi.org/10.1016/j.ifset.2007.07.005>.
- [37] M. Sivakumar, S.Y. Tang, K.W. Tan, Cavitation technology - A greener processing technique for the generation of pharmaceutical nanoemulsions, in: *Ultrason Sonochem*, Elsevier B.V., 2014: pp. 2069–2083. <https://doi.org/10.1016/j.ultsonch.2014.03.025>.
- [38] L. Zhou, W. Zhang, J. Wang, R. Zhang, J. Zhang, Comparison of oil-in-water emulsions prepared by ultrasound, high-pressure homogenization and high-speed homogenization, *Ultrason. Sonochem.* 82 (2022) 105885, <https://doi.org/10.1016/j.ultsonch.2021.105885>.
- [39] J.-P. Franc, J.-M. Michel, *Fundamentals of Cavitation*, Springer, Netherlands, Dordrecht (2005), <https://doi.org/10.1007/1-4020-2233-6>.
- [40] P. Sarkar, G. Ghigliotti, J.P. Franc, M. Fivel, Mechanism of material deformation during cavitation bubble collapse, *J. Fluids Struct.* 105 (2021), <https://doi.org/10.1016/j.jfluidstructs.2021.103327>.
- [41] J. Carpenter, S. George, V.K. Saharan, Low pressure hydrodynamic cavitating device for producing highly stable oil in water emulsion: Effect of geometry and cavitation number, *Chem. Eng. Process. - Process Intensif.* 116 (2017) 97–104, <https://doi.org/10.1016/j.cep.2017.02.013>.
- [42] S. Parthasarathy, T. Siah Ying, S. Manickam, Generation and optimization of palm oil-based oil-in-water (O/W) submicron-emulsions and encapsulation of curcumin using a liquid whistle hydrodynamic cavitation reactor (LWHCR), *Ind. Eng. Chem. Res.* 52 (2013) 11829–11837, <https://doi.org/10.1021/ie4008858>.
- [43] T. Yamamoto, S.V. Komarov, Liquid jet directionality and droplet behavior during emulsification of two liquids due to acoustic cavitation, *Ultrason. Sonochem.* 62 (2020), <https://doi.org/10.1016/j.ultsonch.2019.104874>.
- [44] U. Orthaber, J. Zevnik, R. Petkovšek, M. Dular, Cavitation bubble collapse in a vicinity of a liquid-liquid interface – Basic research into emulsification process, *Ultrason. Sonochem.* 68 (2020), <https://doi.org/10.1016/j.ultsonch.2020.105224>.
- [45] A.H. Thaker, V.V. Ranade, Emulsions using a vortex-based cavitation device: influence of number of passes, pressure drop, and device scale on droplet size distributions, *Ind. Eng. Chem. Res.* (2022), <https://doi.org/10.1021/acs.iecr.2c03714>.
- [46] D. Panda, V.K. Saharan, S. Manickam, Controlled hydrodynamic cavitation: a review of recent advances and perspectives for greener processing, *Processes* 8 (2020), <https://doi.org/10.3390/pr8020220>.
- [47] S.M. Jafari, E. Assadpoor, Y. He, B. Bhandari, Re-coalescence of emulsion droplets during high-energy emulsification, *Food Hydrocoll.* 22 (2008) 1191–1202, <https://doi.org/10.1016/j.foodhyd.2007.09.006>.
- [48] A. Gupta, H.B. Eral, T.A. Hatton, P.S. Doyle, Nanoemulsions: formation, properties and applications, *Soft Matter* 12 (2016) 2826–2841, <https://doi.org/10.1039/C5SM02958A>.
- [49] M. Schlender, A. Spengler, H.P. Schuchmann, High-pressure emulsion formation in cylindrical coaxial orifices: influence of cavitation induced pattern on oil drop size, *Int. J. Multiph. Flow* 74 (2015) 84–95, <https://doi.org/10.1016/j.ijmultiphaseflow.2015.04.004>.
- [50] K.A. Ramisetty, A.B. Pandit, P.R. Gogate, Novel approach of producing oil in water emulsion using hydrodynamic cavitation reactor, *Ind. Eng. Chem. Res.* 53 (2014) 16508–16515, <https://doi.org/10.1021/ie502753d>.
- [51] K.A. Ramisetty, A.B. Pandit, P.R. Gogate, Ultrasound assisted preparation of emulsion of coconut oil in water: understanding the effect of operating parameters and comparison of reactor designs, *Chem. Eng. Process.* 88 (2015) 70–77, <https://doi.org/10.1016/j.cep.2014.12.006>.
- [52] U. Orthaber, M. Dular, R. Petkovšek, Characterization of jet parameters related to cavitation bubble dynamics in a vicinity of a flat liquid-liquid interface, *Exp. Therm Fluid Sci.* 136 (2022), <https://doi.org/10.1016/j.expthermflusci.2022.110651>.
- [53] Y. Zhou, Rayleigh-Taylor and Richtmyer-Meshkov instability induced flow, turbulence, and mixing, I, *Phys Rep* 720–722 (2017) 1–136, <https://doi.org/10.1016/j.physrep.2017.07.005>.
- [54] Y. Zhou, Rayleigh-Taylor and Richtmyer-Meshkov instability induced flow, turbulence, and mixing, II, *Phys Rep* 723–725 (2017) 1–160, <https://doi.org/10.1016/j.physrep.2017.07.008>.
- [55] T. Gotsch, C. Richter, S. Beinert, C. Schilcher, C. Schilde, S. Büttgenbach, A. Kwade, Effect of cavitation on dispersion and emulsification process in high-pressure microsystems (HPMS), *Chem. Eng. Sci.* 144 (2016) 239–248, <https://doi.org/10.1016/j.ces.2016.01.034>.
- [56] P.R. Gogate, A.M. Kabadi, A review of applications of cavitation in biochemical engineering/biotechnology, *Biochem. Eng. J.* 44 (2009) 60–72, <https://doi.org/10.1016/j.bej.2008.10.006>.
- [57] D. Podbevšek, M. Petkovšek, C.D. Ohl, M. Dular, Kelvin-Helmholtz instability governs the cavitation cloud shedding in Venturi microchannel, *Int. J. Multiph. Flow* 142 (2021), <https://doi.org/10.1016/j.ijmultiphaseflow.2021.103700>.
- [58] F. Gallaire, P.T. Brun, Fluid dynamic instabilities: theory & application to pattern forming in complex media, *Philosophical Transactions of the Royal Society A:*

- Mathematical, Phys. Eng. Sci. 375 (2017), <https://doi.org/10.1098/rsta.2016.0155>.
- [59] A. Sarc, T. Stepišnik-Perdih, M. Petkovšek, M. Dular, The issue of cavitation number value in studies of water treatment by hydrodynamic cavitation, *Ultrason. Sonochem.* 34 (2017) 51–59, <https://doi.org/10.1016/j.ultrasonch.2016.05.020>.
- [60] M. Ge, C. Sun, G. Zhang, O. Coutier-Delgosha, D. Fan, Combined suppression effects on hydrodynamic cavitation performance in Venturi-type reactor for process intensification, *Ultrason. Sonochem.* 86 (2022), <https://doi.org/10.1016/j.ultrasonch.2022.106035>.
- [61] P. Pipp, M. Hočevar, M. Dular, Challenges of numerical simulations of cavitation reactors for water treatment – an example of flow simulation inside a cavitating microchannel, *Ultrason. Sonochem.* 77 (2021), <https://doi.org/10.1016/j.ultrasonch.2021.105663>.
- [62] P.F. Pelz, T. Keil, T.F. Gro, The transition from sheet to cloud cavitation, *J. Fluid Mech.* 817 (2017) 439–454, <https://doi.org/10.1017/jfm.2017.75>.
- [63] G. Zhang, I. Khelifa, K. Fezzaa, M. Ge, O. Coutier-Delgosha, Experimental investigation of internal two-phase flow structures and dynamics of quasi-stable sheet cavitation by fast synchrotron x-ray imaging, *Phys. Fluids* 32 (2020), <https://doi.org/10.1063/5.0029963>.
- [64] S. Xu, J. Wang, H. Cheng, B. Ji, X. Long, Experimental study of the cavitation noise and vibration induced by the choked flow in a Venturi reactor, *Ultrason. Sonochem.* 67 (2020), <https://doi.org/10.1016/j.ultrasonch.2020.105183>.
- [65] S. Jahangir, W. Hogendoorn, C. Poelma, Dynamics of partial cavitation in an axisymmetric converging-diverging nozzle, *Int. J. Multiph. Flow* 106 (2018) 34–45, <https://doi.org/10.1016/j.ijmultiphaseflow.2018.04.019>.
- [66] M. Dular, I. Khelifa, S. Fuzier, M. Adama Maiga, O. Coutier-Delgosha, Scale effect on unsteady cloud cavitation, *Exp. Fluids* 53 (2012) 1233–1250, <https://doi.org/10.1007/s00348-012-1356-7>.
- [67] P. Pipp, M. Hočevar, M. Dular, Numerical insight into the Kelvin-Helmholtz instability appearance in cavitating flow, *Appl. Sci. (Switzerland)* 11 (2021), <https://doi.org/10.3390/app11062644>.
- [68] T. Abbasiasl, S. Niazi, A.S. Aghdam, H. Chen, F.Ç. Cebeci, M. Ghorbani, D. Grishenkov, A. Koşar, Effect of intensified cavitation using poly(vinyl alcohol) microbubbles on spray atomization characteristics in microscale, *AIP Adv.* 10 (2020), <https://doi.org/10.1063/1.5142607>.
- [69] D. Podbevšek, G. Ledoux, M. Dular, Investigation of hydrodynamic cavitation induced reactive oxygen species production in microchannels via chemiluminescent luminol oxidation reactions, *Water Res.* 220 (2022), <https://doi.org/10.1016/j.watres.2022.118628>.
- [70] T.T. Clark, Y. Zhou, Self-similarity of two flows induced by instabilities, *Phys. Rev. E* 68 (2003) 66305, <https://doi.org/10.1103/PhysRevE.68.066305>.
- [71] J. Huang, L. Sun, M. Du, Z. Mo, L. Zhao, A visualized study of interfacial behavior of air–water two-phase flow in a rectangular Venturi channel, *Theor. Appl. Mech. Lett.* 8 (2018) 334–344, <https://doi.org/10.1016/j.taml.2018.05.004>.
- [72] E.G. Chatzi, C. Kiparissides, Dynamic simulation of bimodal drop size distributions in low-coalescence batch dispersion systems, *Chem. Eng. Sci.* 47 (1992) 445–456, [https://doi.org/10.1016/0009-2509\(92\)80032-8](https://doi.org/10.1016/0009-2509(92)80032-8).